

Subnanometer traceability of localization microscopy

CRAIG R. COPELAND,¹ RONALD G. DIXSON,¹ ADAM L. PINTAR,² B. ROBERT ILIC,^{1,3}
AND SAMUEL M. STAVIS^{1,*}

¹Microsystems and Nanotechnology Division, ²Statistical Engineering Division, ³CNST NanoFab,
National Institute of Standards and Technology, Gaithersburg, MD, USA

*Corresponding author: samuel.stavis@nist.gov

In localization microscopy, subnanometer precision is possible but supporting accuracy is challenging, and no study has demonstrated reliable traceability to the International System of Units (SI). To do so, we measure the positions of nanoscale apertures in a reference array by traceable atomic-force microscopy, creating a master standard. We perform correlative measurements of this standard by optical microscopy, correcting position errors from optical aberrations by a Zernike calibration. We establish an uncertainty field due to localization errors and scale uncertainty, with regions of position traceability to within a 68 % coverage interval of ± 1.0 nm. These results enable localization metrology with high throughput, which we apply to measure working standards, validating the subnanometer accuracy of lithographic pitch.

Localization microscopy has left the diffraction limit of a few hundred nanometers in the rearview optics, with uncertainty from the random effect of photon shot noise ranging down to one nanometer and below [1-3]. Systematic effects, however, can be orders of magnitude larger and can vary unpredictably across the imaging field [3]. Correction of such effects requires comprehensive calibration of optical microscopes [3-6], which is uncommon, leading to a common discrepancy of precision and accuracy, and potential overconfidence in localization data. Moreover, no previous study has established a continuous chain of calibrations for localization microscopy that is reliably traceable to the International System of Units (SI). This fundamental issue is becoming more important as localization microscopy matures, requiring not only novel methods but also reliable quantities for meaningful comparison.

A calibration is only as good as the standard providing a reference. Common, if unofficial, standards for localization microscopy include fluorescent particles [5, 7, 8], molecular nanostructures [9, 10], and nanoscale apertures [3, 11]. Of these, aperture arrays feature stability, reusability, flexibility of both design from the top down and use under different imaging conditions, and accessibility for correlative microscopy to establish traceability. In a previous study, we fabricated aperture arrays by electron-beam lithography and tested aperture placement [3]. Two lithography systems each used two interferometers to control stage positions and correct for electron-optical aberrations within the patterning process. By localizing apertures and comparing placements by the two systems, we estimated a mean distance between apertures that differed by one part in five thousand, or approximately 1 nm, and random placement errors of approximately 2 nm. Although the implication was placement accuracy at the nanometer scale, these test results were insufficient for a chain or claim of traceability.

Even with a standard in hand, there are at least four challenges that impede traceability of localization microscopy. The first is matching the system optics, imaging conditions, object positions, and localization analyses between calibration and experiment [3]. Any inconsistency can compromise accuracy and undermine reliability, compounding the

second challenge of calibrating the scale factor, or magnification, of an optical microscope with low uncertainty, such as by limiting the applicability of calibration data from microstructure arrays that diverge from the typical experimental context of localization microscopy [10, 12, 13]. These limits also pertain to the third challenge of sampling the imaging field in two or three dimensions with nanostructures that are suitable for localization microscopy and that probe field nonuniformity, ideally with uniform sampling at the scale from one to ten wavelengths [5]. The fourth challenge is making optimal use of calibration data to minimize uncertainty. No previous study has met all of these challenges.

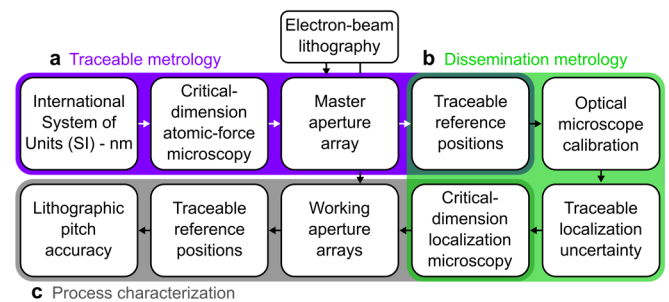


Fig. 1. Overview. A calibration chain from (a) traceable metrology, to (b) dissemination metrology, to (c) process characterization.

In the present study, we meet these challenges to establish a reliable calibration chain from the SI to localization microscopy, achieving subnanometer traceability and closing the loop of fabricating standards (Fig. 1). We begin by measuring aperture positions by critical-dimension atomic-force microscopy [14, 15]. This method is traceable to the SI through interferometric calibrations and transfer standards [16, 17], yielding a master standard (Fig. 1a). Correlative measurements by localization microscopy enable optical calibration [3]. Statistical models lead

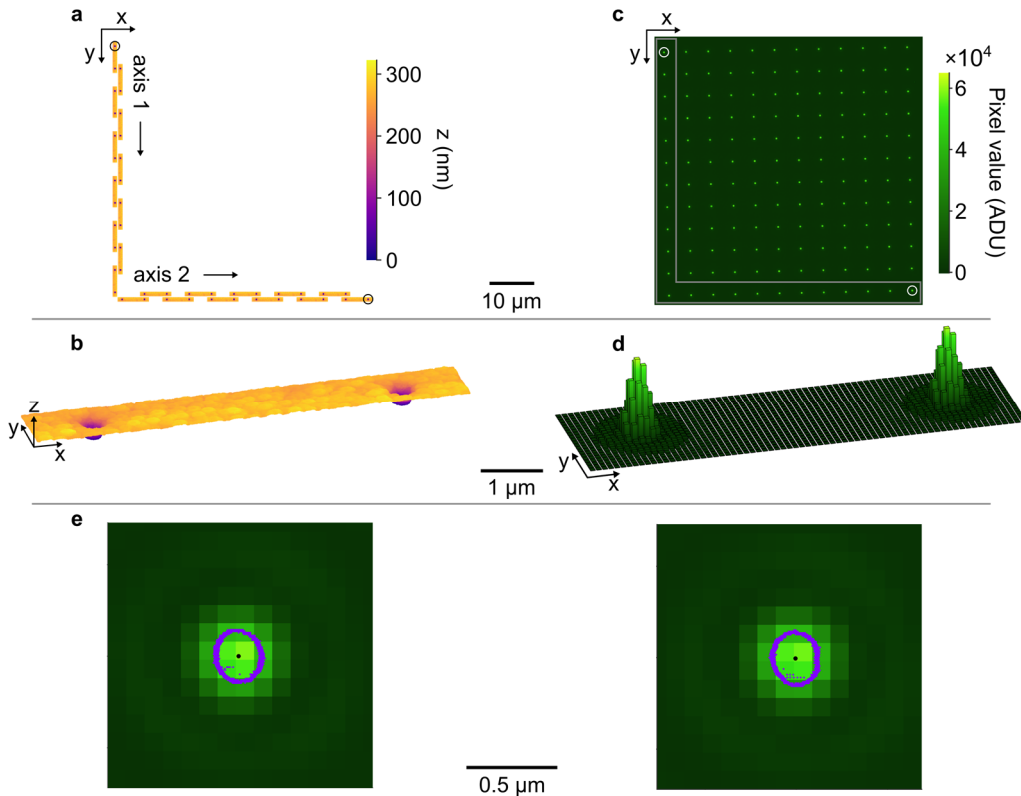


Fig. 2. Correlative microscopy. (a-b) Atomic-force micrographs showing (a) separate images of 22 pairs of apertures and (b) an image of a representative pair of apertures. (c-d) Optical micrographs showing (c) the entire aperture array and (d) an image of the same representative pair of apertures. The gray outline in (c) indicates the same apertures as in (a). Circles in (a, c) indicate two corner apertures. (e) Correlative micrographs showing the direct overlay of image data from the two microscopy methods. Black dots mark the positions resulting from localization analyses. Position uncertainties are smaller than the black dots.

to the concept of an uncertainty field, shifting the paradigm in localization microscopy from precision to accuracy [3] and now traceability (Fig. 1b). Critical-dimension localization microscopy enables characterization of multiple aperture arrays with high throughput. A statistical meta-analysis validates lithographic accuracy, closing the loop of producing working standards for dissemination (Fig. 1c). Terms and symbols are in Table S1.

We begin with one of the aperture arrays from our previous test [3], for which we had designed a pitch of 5000 nm and found a deviation of approximately 1 nm. We presently image 21 pairs of adjacent apertures in triplicate, and one pair in duplicate, by critical-dimension atomic-force microscopy (Fig. 2a-b) (Table S1) (Table S2), sampling along the periphery of the array to subject the accuracy of our optical calibration to a stress test [3]. The two axes of the atomic-force microscope scan independently. We use each axis to image 11 different aperture pairs, probing the aperture sidewalls with a flared tip, and measuring distance with a resolution of less than 0.1 nm and a relative uncertainty of approximately one part in 10^4 [14-17]. Uncertainties are 68 % coverage intervals (Note S1) (Table S3). This uncertainty results from calibration of the mean scale factor and correction of the non-uniform scale factor due to scanning non-linearity (Fig. S1). We analyze the sidewall positions ranging from 30 nm to 95 nm above the zero plane of the silica substrate (Fig. S2), assuming that this nearly vertical region determines the transmission of light through the apertures. We compare elliptical models and centroid analyses of the sidewall positions to localize each aperture. Least-squares fits of elliptical models with uniform weighting smooth the scatter of the

sidewall positions, reducing the pooled standard deviation of the distance between pairs of adjacent apertures from 1.50 nm to 0.98 nm, so we proceed with this analysis.

We develop complementary statistical models to analyze the distance data and enable evaluation of different components of uncertainty (Note S2) (Table S1). Fixed-effect models estimate the magnitude of localization errors in optical microscopy [3]. An autoregressive model treats the correlation of adjacent aperture pairs in atomic-force microscopy (Fig. 2a). The comparable results of the two models are similar. The fixed-effect model for atomic-force microscopy yields a mean distance of $5000.72 \text{ nm} \pm 0.24 \text{ nm}$ for axis 1, $5000.69 \text{ nm} \pm 0.06 \text{ nm}$ for axis 2, and $5000.71 \text{ nm} \pm 0.13 \text{ nm}$ for both axes. These uncertainties account for variability from replicate measurements and from sampling the 22 pairs of apertures (Table S2). The propagation of scale uncertainty (Table S3) results in a traceable mean distance of $5000.71 \text{ nm} \pm 0.54 \text{ nm}$. Although this pitch of the master standard is near to nominal, tests of more standards are necessary to establish lithographic accuracy, which we revisit.

We image the entire array by optical microscopy near best focus (Fig. 2c-d), with 1000 replicates (Table S2) [3]. The sample orientation yields aperture distances that are in near alignment with the x and y axes of the optical microscope, corresponding to axes 2 and 1 of the atomic-force microscope (Fig. 2). We localize the apertures, correlate the position data (Fig. 2e), and calibrate our optical microscope by our previous methods [3] with a key modification. The mean distance between apertures from atomic-force microscopy, rather than the nominal pitch from electron-beam lithography, defines the pitch of an ideal

array in a similarity transformation, yielding position errors that a Zernike polynomial model corrects [3]. For 144 apertures in a field of $3600 \mu\text{m}^2$, a Noll index of 52 for x and 48 for y minimizes root-mean-square deviations of distance between the same aperture pairs by the two microscopy methods. This calibration yields mean magnification and corrects the effects of distortion, among other aberrations (Fig. 3).

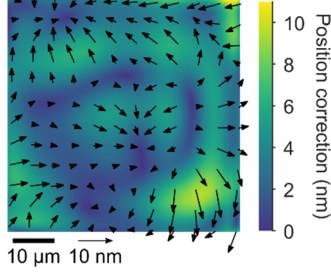


Fig. 3. Optical microscope calibration. Vector plot and color map showing a position correction for optical microscopy, after calibration of mean magnification and image pixel size.

To test the calibration, we develop another fixed-effect statistical model to analyze the distances between aperture pairs for optical microscopy, and combine the models to analyze the distance deviations between the two microscopy methods (Table S1) (Note S2). The distance values are in evident agreement (Fig. 4). We confirm that the mean deviation is zero (Table S2) and that the variance of the experimental deviations is consistent with that of the model predictions. The models define total variances (Eq. 1) $\sigma_{D_{AFM}}^2 = \sigma_{\delta_{AFM}}^2 + \sigma_{d_{AFM}}^2/n_{D_{AFM}}$ for atomic-force microscopy and (Eq. 2) $\sigma_{D_{OM}}^2 = \sigma_{\delta_{OM}}^2 + \sigma_{d_{OM}}^2/n_{D_{OM}}$ for optical microscopy (Note S2). We divide the variances from replicates, $\sigma_{d_{OM}}^2$ and $\sigma_{d_{AFM}}^2$, by the sample sizes, since we average distances over replicates. The variances $\sigma_{\delta_{AFM}}^2$ and $\sigma_{\delta_{OM}}^2$ are from localization errors, such as from non-uniform scale or deviations of aperture images and localization models. For optical microscopy, $\sigma_{d_{OM}}/\sqrt{2}$ is the common metric of empirical localization precision and $\sigma_{\delta_{OM}}/2$ is the variance of position from localization errors that are unobservable in temporal replicates [3] (Table S4). Assuming independence of random effects, the sample variance of distance deviations is Eq. 1 plus Eq. 2, (Eq. 3) $\sigma_{D_{OM-D_{AFM}}}^2 = \sigma_{\delta_{OM}}^2 + \sigma_{d_{OM}}^2/n_{D_{OM}} + \sigma_{\delta_{AFM}}^2 + \sigma_{d_{AFM}}^2/n_{D_{AFM}}$. Pooling the sample variances of the replicate measurements yields values for $\sigma_{d_{AFM}}^2$ and $\sigma_{d_{OM}}^2$, separately for each axis of the atomic-force microscope, due to the higher variability of axis 1 from a control algorithm to improve sidewall tracking (Fig. 4). We estimate $\sigma_{\delta_{AFM}}^2$ for each axis and solve for $\sigma_{\delta_{OM}}^2$, having estimates of all other terms (Table S5) (Table S6).

For atomic-force microscopy, replication statistics dominate the variance for both axes, whereas $\sigma_{\delta_{AFM}}$ is negligible (Fig. S1) (Table S6). For optical microscopy, averaging $n_{D_{OM}} = 1000$ replicates, with 0.6×10^6 signal photons per image, reduces $\sigma_{d_{OM}}^2/n_{D_{OM}}$ to a negligible value (Table S5) [18]. The resulting solutions for $\sigma_{\delta_{OM}}$, in both the x and y directions, agree with those from our previous study with a larger field of $40000 \mu\text{m}^2$ (Table S6) [3], validating the localization errors and indicating that they are spatially random and independent of field area. The effect of fabrication precision on the Zernike model causes localization errors of less than 0.1 nm [3], with the remainder motivating further study.

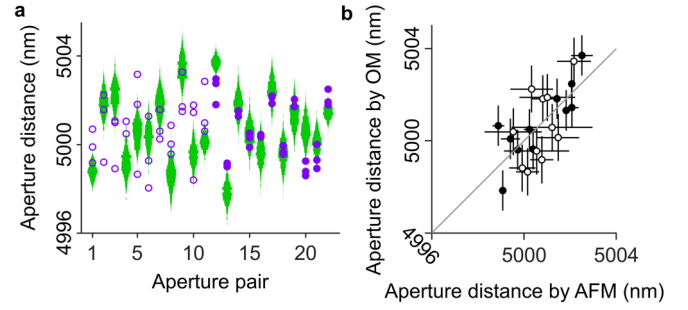


Fig. 4. Aperture distance measurements. **(a)** Plot showing the correlation of aperture distances from (purple circles, hollow circles are axis 1, solid circles are axis 2) atomic-force microscopy (AFM) and (green violin histograms) optical microscopy (OM). **(b)** Plot showing the correlation of distances for the different measurements, with a reduction of the data in (a) to mean values and 68 % coverage intervals in (b).

For optical microscopy, to quantify the lower limit of traceable position uncertainty, $\sigma_{D_{OM}}$ sums in quadrature with the absolute uncertainty of scale. For the uncertainty of position relative to a reference point that does not require localization analysis, such as the center position of an imaging sensor of a stable microscope, values of $\sigma_{D_{OM}}$ reduce by a factor of $\sqrt{2}$, Eq. (4)

$$u_{D_{x,y}}^{OM} = \sqrt{\left(\sigma_{D_{x,y}}^{OM}/\sqrt{2}\right)^2 + \left(D_{x,y}^{OM} \times \sigma_s\right)^2}$$
 (Fig. 5) (Table S3) (Table S6), where D_x^{OM} is the distance in the x direction from a reference point, with an analogous expression for the y direction, and σ_s is the relative uncertainty of scale. A general expression for the uncertainty of Euclidean distance D^{OM} , including localization uncertainty for two points, is in Note S3. The first term in Eq. 4 is constant, whereas the second term scales with distance (Fig. 5a). This is characteristic of coordinate-measuring machines, closing the gap between such systems and ordinary microscopes, and emphasizing the need to calibrate scale factor and propagate its uncertainty in localization microscopy. The common absence of this calibration causes unidentified errors and underestimates of uncertainty. Eq. (4) and its analogue in the y direction describe an uncertainty field with two regions in which positions have subnanometer traceability (Fig. 5b). In the inner region, the maximum uncertainty is less than ± 1.0 nm across an area of $150 \mu\text{m}^2$. In the outer region, the mean uncertainty is less than ± 1.0 nm across an area of $304 \mu\text{m}^2$. Notably, both regions are asymmetric, and the field exhibits complex variation around the center due to the different values of $\sigma_{\delta_x^{OM}}$ and $\sigma_{\delta_y^{OM}}$ (Fig. 5).

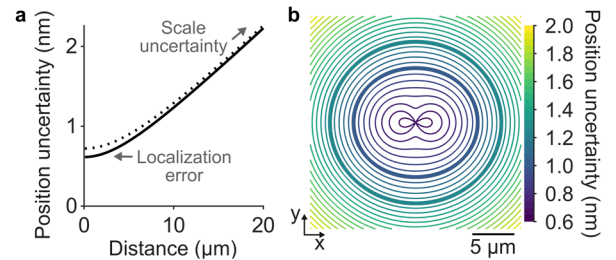


Fig. 5. Traceable position uncertainty. **(a)** Plot showing position uncertainty of optical microscopy $u_{D_{x,y}}^{OM}$ as a function of distance $D_{x,y}^{OM}$ from a reference point for the (solid) x and (dash) y directions. **(b)** Contour plot showing the corresponding uncertainty field for position in reference to the field center. Two bold contours are limits of (inner) maximum and (outer) mean uncertainty of less than ± 1.0 nm. Contour intervals are 0.05 nm.

In a final test of the two microscopy methods, we measure the diagonal distance between two corner apertures (Fig. 2a, c), neglecting the common uncertainty of scale to isolate other components of uncertainty. For atomic-force microscopy, assuming that the array axes are orthogonal and that off-axis effects of fabrication precision are negligible, summation of distances between the intermediate 22 aperture pairs (Fig. 2a) yields $77792.76 \text{ nm} \pm 1.94 \text{ nm}$, with random effects dominating. For optical microscopy, direct localization of only the two corner apertures (Fig. 2c) yields $77792.05 \text{ nm} \pm 0.95 \text{ nm}$, with systematic effects dominating. Thus, the critical dimensions are in subnanometer agreement, validating axis orthogonality and localization analysis, and showing that optical localization yields half the uncertainty from components that are not common to both methods and higher throughput by a factor of 10^5 .

We apply critical-dimension localization microscopy to rapidly characterize five more aperture arrays (Table S7). A statistical meta-analysis yields a consensus mean pitch of $4999.34 \text{ nm} \pm 1.00 \text{ nm}$, an estimate of pitch variability of 2.25 nm , and a prediction interval of $4999.40 \text{ nm} \pm 2.34 \text{ nm}$ (Note S4). These results validate the subnanometer accuracy of mean pitch and, due to our deliberate variation of process parameters, provide a conservative estimate of the reliability of producing replicate standards by electron-beam lithography.

In conclusion, we establish a firm foundation for traceable localization with subnanometer uncertainty. This new capability is fundamental as localization microscopy matures into a quantitative phase, requiring not only novel methods, but also reliable quantities for meaningful comparisons across studies.

We perform the first localization correlation of aperture arrays by atomic-force and optical microscopy, yielding a master standard for optical calibration. The positions correlate to within a few nanometers (Table S2), which is interesting considering that the aperture sidewalls are rough at a much larger scale of tens of nanometers. These results open the door to traceable correlations of surface structure and optical signal, extending down toward the atomic scale, across a wide field.

We establish the concept of an uncertainty field in localization microscopy, shifting the paradigm from a focus on precision to a broader understanding of accuracy [3] and now traceability, with a critical limit due to scale calibration. The impact of scale uncertainty depends on localization precision and field area. For super-resolution imaging, a count of 10^3 to 10^4 signal photons per fluorophore image limits localization precision to a few tens of nanometers within a field area of a few square micrometers. In this context, errors from scale uncertainty can be negligible. However, a stable and intense emitter can yield 10^6 signal photons per image, with localization precision extending into the picometer scale by averaging replicates (Table S6) [5, 18]. In this context, errors from scale uncertainty, which increase with distance, can be dominant across virtually any field area.

Our approach extends a new level of traceability to ordinary optical microscopes in the field, upgrading them into metrology systems with high throughput. In this way, we develop and apply critical-dimension localization microscopy to test multiple aperture arrays, validating lithographic accuracy at the subnanometer scale. Future studies could optimize the lithography process and establish statistical process control to produce working standards with high quality and efficiency for dissemination, potentially without the need for individual characterization. Finally, our standards are integrable for *in situ* calibration of beam placement and emitter position [19].

Funding sources and acknowledgments. We acknowledge John Kramar for an insightful review. We acknowledge funding from the NIST Innovations in Measurement Science Program and the NIST Office of Reference Materials.

Disclosures. The authors declare no conflict of interest.

Supplemental Document. See <link> for supporting content.

References

1. A. Yildiz, J. N. Forkey, S. A. McKinney, T. Ha, Y. E. Goldman, and P. R. Selvin, *Science* **300**, 2061 (2003).
2. A. Pertsinidis, Y. Zhang, and S. Chu, *Nature* **466**, 647-651 (2010).
3. C. R. Copeland, J. Geist, C. D. McGray, V. A. Aksyuk, J. A. Liddle, B. R. Ilic, and S. M. Stavis, *Light: Science & Applications* **7**, 1-15 (2018).
4. C. R. Copeland, B. R. Ilic, and S. M. Stavis, *Frontiers in Optics*, (Optical Society of America, 2019), FM1C. 3.
5. C. R. Copeland, C. D. McGray, B. R. Ilic, J. Geist, and S. M. Stavis, *Nature Communications* **12**, 3925 (2021).
6. M. Bierbaum, B. D. Leahy, A. A. Alemi, I. Cohen, and J. P. Sethna, *Physical Review X* **7**, 041007 (2017).
7. T. Yan, C. Richardson, M. Zhang, and A. Gahlmann, *Biophysical Journal* **116**, 282a (2019).
8. Y. Li, M. Mund, P. Hoess, J. Deschamps, U. Matti, B. Nijmeijer, V. J. Sabinina, J. Ellenberg, I. Schoen, and J. Ries, *Nature Methods* **15**, 367 (2018).
9. J. V. Thevathasan, M. Kahnwald, K. Cieřliński, P. Hoess, S. K. Peneti, M. Reitberger, D. Heid, K. C. Kasuba, S. J. Hoerner, Y. Li, Y.-L. Wu, M. Mund, U. Matti, P. M. Pereira, R. Henriques, B. Nijmeijer, M. Kueblbeck, V. J. Sabinina, J. Ellenberg, and J. Ries, *Nature Methods* **16**, 1045-1053 (2019).
10. M. Raab, I. Jusuk, J. Molle, E. Buhr, B. Bodermann, D. Bergmann, H. Bosse, and P. Tinnefeld, *Scientific Reports* **8**, 1780 (2018).
11. A. v. Diezmann, M. Y. Lee, M. D. Lew, and W. E. Moerner, *Optica* **2**, 985-993 (2015).
12. P. Ekberg and L. Mattsson, *Measurement Science and Technology* **29**, 035005 (2018).
13. X. Dai, H. Xie, C. Li, Z. Wu, and H. Geng, *Optical Engineering* **52**, 114102-114102 (2013).
14. Y. Martin and H. K. Wickramasinghe, *Applied Physics Letters* **64**, 2498-2500 (1994).
15. L. Mininni, J. Foucher, and P. Faurie, *Metrology, Inspection, and Process Control for Microlithography XXI*, (International Society for Optics and Photonics, 2007), 651830.
16. R. G. Dixson, N. G. Orji, C. McGray, J. E. Bonevich, and J. C. Geist, *Journal Of Micro/Nanolithography, MEMS, and MOEMS* **11**, 011006 (2012).
17. J. A. Kramar, R. Dixson, and N. G. Orji, *Measurement Science and Technology* **22**, 024001 (2010).
18. C. R. Copeland, C. D. McGray, J. Geist, J. A. Liddle, B. R. Ilic, and S. M. Stavis, *Optical MEMS and Nanophotonics (OMN), 2017 International Conference on*, (IEEE, 2017), 1-2.
19. K.-T. Liao, A. C. Madison, A. L. Pintar, B. R. Ilic, C. R. Copeland, and S. M. Stavis, arXiv preprint arXiv:2101.03881 (2020).

Subnanometer traceability of localization microscopy: supplemental document

INDEX

Table S1. Terms and symbols

Table S2. Aperture pair distances

Note S1. Uncertainty evaluation and expression

Table S3. Microscopy scale uncertainty

Fig. S1. Atomic-force microscope scale correction

Fig. S2. Representative sidewall data

Note S2. Statistical models

Table S4. Distance uncertainty observability

Fig. S3. Autocorrelation analyses

Table S5. Distance deviation variances

Table S6. Distance uncertainty evaluation

Note S3. Distance uncertainty for optical microscopy

Table S7. Master and working standards

Note S4. Lithographic pitch accuracy

References

Table S1. Terms and symbols

Term	Symbol
General distance analysis	
True distance between two points	Δ
Experimental measurement of distance between two points by AFM or OM	D^{AFM}, D^{OM}
Experimental measurement of distance between two points in the x or y direction by OM	D_x^{OM}, D_y^{OM}
Uncertainty of D^{OM}	$u_{D^{OM}}$
Uncertainty of D_x^{OM} or D_y^{OM} between one localization result and a reference position	$u_{D_x^{OM}}, u_{D_y^{OM}}$
Uncertainty of D_x^{OM} or D_y^{OM} between two localization results	$u_{D_x^{OM}}^{\parallel}, u_{D_y^{OM}}^{\parallel}$
Scale factor for OM	S
Scale uncertainty for OM	σ_S
Aperture pair analysis	
Aperture pair index	i
Replicate measurement index	j
Number of replicate measurements of aperture pair distance by AFM	$n_{D^{AFM}}$
Experimental measurement of aperture pair distance by AFM	$D_{ij}^{AFM} = \Delta_i + d_{ij}^{AFM} + \delta_i^{AFM}$
Random error of distance that is observable between replicates for AFM	d_{ij}^{AFM}
Variance of d_{ij}^{AFM} assuming the same for each pair and replicate, and dividing by $n_{D^{AFM}}$	$\sigma_{d^{AFM}}^2 / n_{D^{AFM}}$
Random error of distance that is unobservable between replicates for AFM	δ_i^{AFM}
Variance of δ_i^{AFM} assuming the same for each pair	$\sigma_{\delta^{AFM}}^2$
Variance of D^{AFM}	$\sigma_{D^{AFM}}^2 = \sigma_{\delta^{AFM}}^2 + \sigma_{d^{AFM}}^2 / n_{D^{AFM}}$
Number of replicate measurements of aperture pair by OM	$n_{D^{OM}}$
Experimental measurement of aperture pair distance by OM	$D_{ij}^{OM} = \Delta_i + d_{ij}^{OM} + \delta_i^{OM}$
Random error of distance that is observable between replicates for OM	d_{ij}^{OM}
Variance of d_{ij}^{OM} assuming the same for each pair and replicate, and dividing by $n_{D^{OM}}$	$\sigma_{d^{OM}}^2 / n_{D^{OM}}$
Random error of distance that is unobservable between replicates for OM	δ_i^{OM}
Variance of δ_i^{OM} assuming the same for each pair	$\sigma_{\delta^{OM}}^2$
Variance of D^{OM}	$\sigma_{D^{OM}}^2 = \sigma_{\delta^{OM}}^2 + \sigma_{d^{OM}}^2 / n_{D^{OM}}$
Distance deviation after averaging over replicates	$D_i^{OM} - D_i^{AFM}$
Variance of distance deviations over pairs	$\sigma_{D^{OM} - D^{AFM}}^2$

AFM is atomic-force microscopy. OM is optical microscopy.

For clarity of nomenclature, we include only symbols that appear in this study. For example, D_x^{AFM} does not appear.

For completeness, $u_{D_x^{OM}} = u_{D_x^{OM}}^1$ and $u_{D_y^{OM}} = u_{D_y^{OM}}^1$, which we revisit in Note S3. For clarity, we simply this notation in the main text.

A dot symbol for j in a subscript denotes an average over replicate measurements.

Additional information and discussions of these quantities are in Table S4, Note S2, and Note S3.

Table S2. Aperture pair distances

Aperture pair i	Distance by AFM D_{ij}^{AFM} (nm)					Distance by OM D_{ij}^{OM} (nm)		Deviation $D_{i.}^{OM} - D_{i.}^{AFM}$ (nm)
	D_{i1}^{AFM}	D_{i2}^{AFM}	D_{i3}^{AFM}	$D_{i.}^{AFM}$	$\sigma_{D_{ij}^{AFM}}$	$D_{i.}^{OM}$	$\sigma_{D_{ij}^{OM}}$	
1	4999.89	4999.18	5000.70	4999.93	0.76	4998.82	0.35	-1.11
2	4999.21	5002.24	5001.58	5001.01	1.60	5001.88	0.53	0.87
3	5001.08	5001.00	4998.91	5000.33	1.23	5002.24	0.57	1.91
4	5000.49	-	5001.05	5000.77	0.40	4999.18	0.56	-1.59
5	5001.82	5003.17	4998.66	5001.22	2.31	5000.58	0.57	-0.63
6	4999.28	4998.04	5001.28	4999.53	1.63	5000.39	0.57	0.86
7	5001.58	5000.25	5000.61	5000.82	0.69	5001.82	0.59	1.01
8	4999.57	5000.87	5000.02	5000.15	0.66	4998.65	0.59	-1.50
9	5001.71	5001.50	5003.28	5002.16	0.97	5003.45	0.57	1.29
10	5001.45	5001.78	4998.40	5000.55	1.86	4999.56	0.53	-0.99
11	5002.85	5000.61	5000.98	5001.48	1.20	5000.14	0.33	-1.34
12	5002.97	5001.81	5002.76	5002.51	0.62	5003.71	0.27	1.20
13	4999.00	4999.16	4999.07	4999.08	0.08	4997.84	0.46	-1.24
14	5001.27	5001.53	5001.48	5001.43	0.14	5001.83	0.55	0.40
15	5000.31	5000.52	4999.87	5000.24	0.33	5000.49	0.55	0.26
16	5000.37	5000.46	5000.34	5000.39	0.06	4999.64	0.55	-0.75
17	5002.16	5002.20	5001.85	5002.07	0.19	5002.47	0.54	0.40
18	4999.57	4999.66	4999.96	4999.73	0.20	4999.61	0.57	-0.12
19	5001.71	5002.04	5001.73	5001.83	0.19	5001.32	0.57	-0.51
20	4999.26	4998.60	4998.79	4998.88	0.34	5000.65	0.56	1.77
21	5000.01	4998.92	4999.30	4999.41	0.55	5000.08	0.48	0.67
22	5001.79	5002.50	5001.93	5002.07	0.38	5001.44	0.27	-0.63

Aperture pairs 1 to 11 correspond to AFM axis 1 and OM y axis.

Aperture pairs 12 to 22 correspond to AFM axis 2 and OM x axis.

Distance by OM results from 1000 replicate measurements.

Note S1. Uncertainty evaluation and expression

We evaluate and express uncertainty using multiple methods that are fit for our particular purposes, drawing from three sets of guidelines that are in current use at the National Institute of Standards and Technology (NIST) [1-3]. Moreover, we aim to express uncertainty in a way that is clear to both localization microscopists and dimensional metrologists, meriting further discussion. In this regard, there are at least three issues to consider.

First, we consider an ideal measurement of position along a single axis by optical microscopy, featuring only the effect of shot noise from a large number of signal photons on localization uncertainty. The localization precision [4, 5] is equal to the standard deviation σ of a normal distribution with a mean value μ . From n independent measurements, σ is approximately equal to the sample standard deviation s . Per the original guidelines of NIST [1], this statistical analysis is exemplary of a Type A evaluation of an uncertainty component. For replicate measurements following a normal distribution, the original guidelines [1] refer to a standard uncertainty $u = s$. This term is ambiguous, however, as we revisit. Multiplication of u by a coverage factor k yields an expanded uncertainty $U = ku$, corresponding to a confidence interval. In the context of localization microscopy, the natural value of the coverage factor is $k = 1$, although expressions of coverage factors are uncommon. For $n \gtrsim 30$, $k = 1$ yields a 68 % confidence interval of $\pm(U = u \approx \sigma)$. In the context of dimensional metrology, higher values of k are common in expressions of greater confidence, such as $k = 2$ to express a 95 % confidence interval of $\pm(U = 2u \approx 2\sigma)$ for $n \gtrsim 30$. Regardless of the low coverage, a 68 % confidence interval maximizes the overlap of knowledge and minimizes the effort to compare uncertainties between localization microscopy and dimensional metrology.

The second issue is that, depending on the context, the standard uncertainty u can correspond either to the standard deviation σ of a distribution, as in the preceding example, or to the standard error ε of the mean μ of a distribution, $\varepsilon_\mu = \sigma/\sqrt{n}$, or even to the standard error ε of the standard deviation σ of a distribution, ε_σ , as Ref. [6] describes. The first two contexts are the most relevant in our study. To avoid this ambiguity, we subsequently eschew the terms standard uncertainty and expanded uncertainty, which are common in dimensional metrology. Instead, we proceed to reporting confidence intervals, using a Student t distribution with the appropriate number of degrees of freedom $\nu = n - 1$ for each measurement result and expression of uncertainty. For $\nu \gtrsim 30$, the Student t distribution is approximately equal to the standard normal distribution. The value of k depends on n and, such as for triplicate and duplicate measurements, can significantly exceed unity to yield a confidence interval of approximately 68 %. We use the exact version of the approximation in Eq. S1 [6] for $\nu < 30$.

The third issue is that our evaluation of total uncertainty includes Type B evaluations of uncertainty components resulting from systematic effects, such that the term confidence interval, as statisticians use it, is no longer applicable [1], but the term coverage interval is still applicable [2, 3].

Considering these three issues, we report all uncertainties as 68 % coverage intervals, accounting for the number of degrees of freedom and type of distribution, and including one insignificant figure in some quantities to avoid significant rounding errors.

Table S3. Microscopy scale uncertainty

Uncertainty component	Relative value
Uncertainty of transfer standard for AFM scale calibration	6.75×10^{-5}
Variability of replicate calibrations of AFM scale	7.90×10^{-5}
Variability of pitch estimate from AFM measurements	2.60×10^{-5}
Total uncertainty of scale for calibration and application of OM	$\sigma_S = 1.07 \times 10^{-4}$

Scale uncertainties involve Type A and Type B evaluations of several components. We approximate the total uncertainty of scale for calibration and application of OM as a 68 % coverage interval for a normal distribution.

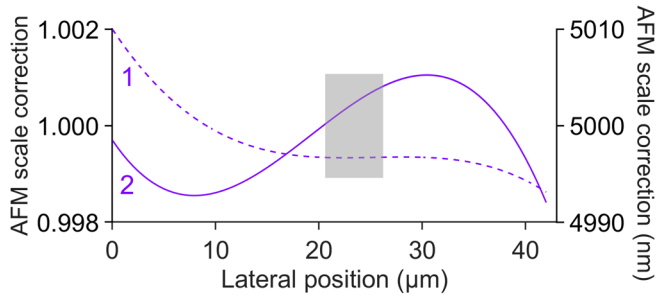


Fig. S1. Atomic-force microscope scale correction. Plot showing scale corrections for (dash line) axis 1 and (solid line) axis 2. The gray box indicates the region of interest of the imaging field. For axis 1, the scale factor is nearly constant in the region of interest, yielding a negligible value of $\sigma_{\delta AFM}$ (Table S6). For axis 2, the scale factor varies nearly linearly in the region of interest, and we use a scale correction from near the mid-point of the aperture pairs. The repeatability of sample positioning is within $0.2 \mu\text{m}$, yielding a larger but still negligible value of $\sigma_{\delta AFM}$ (Table S6).

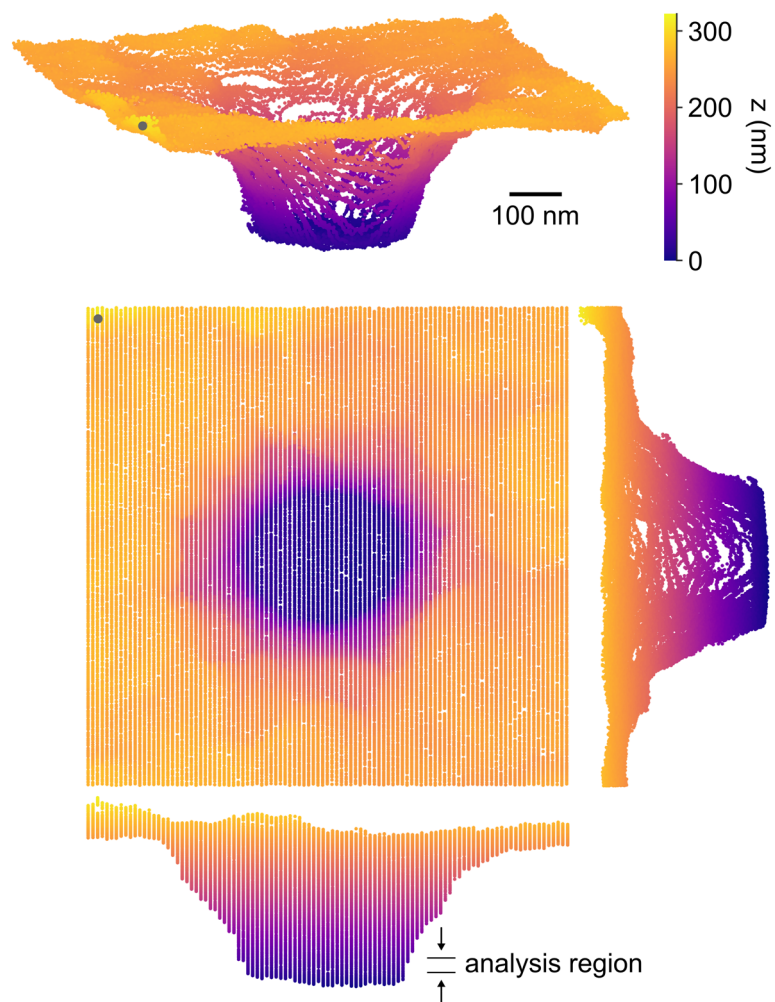


Fig. S2. Representative sidewall data. Atomic-force micrograph showing a representative aperture in different perspectives. The data structure results from axis 2 of the atomic-force microscope. Gray dots indicate the same corner of the micrograph. Black arrows indicate the sidewall region that we select for localization analysis.

Note S2. Statistical models

We develop two statistical models to analyze aperture pair distances. The models are complementary and yield consistent results. Both models account for variability that is observable within each set of measurement results from the two microscopy methods. The fixed-effect linear model accounts for additional variability that is unobservable within each set of measurement results, due to localization errors in both atomic-force microscopy and in optical microscopy. We can independently estimate the former errors and solve for the latter errors in a comparison of the two sets of measurement results. The autoregressive–moving-average model incorporates aperture placement as another component of uncertainty, yielding slightly larger 68 % coverage intervals. Neither statistical model accounts for uncertainty due to scale, which is common to both models but does not cause observable variability (Table S1, Table S4). We propagate the uncertainty of scale subsequently (Note 3).

Fixed-effect linear model

For atomic-force microscopy, the distance from replicate measurement j of aperture pair i is $D_{ij}^{AFM} = \Delta_i + d_{ij}^{AFM} + \delta_i^{AFM}$, where Δ_i is the true distance between aperture pair i , d_{ij}^{AFM} is a random error that is observable between replicate measurements of aperture pair i , and δ_i^{AFM} is a random error that is unobservable between replicate measurements of aperture pair i . It is necessary to allow each aperture pair to have its own true distance Δ , because for two adjacent pairs, if the second aperture is closer to the first aperture, then it is likely further from the third aperture. Such a correlation suggests an alternate analysis by an autoregressive–moving-average model, as we describe subsequently. For each axis, the mean distance is $\frac{1}{11} \sum_{i=1}^{11} \Delta_i + \delta_i^{AFM}$. For the available data, it is not possible to estimate both Δ_i and δ_i^{AFM} , but it is possible to estimate their sum. Additional data allows estimation of the magnitudes of the δ_i^{AFM} . We take as an estimate of the array pitch the average of the mean distances from each axis, neglecting the possibility of a correlation of those mean distances because they share a corner aperture. It is reasonable to neglect this possible correlation because, as we describe in the next section, higher variability of replicate measurements obscures correlations between adjacent pairs of apertures along axis 1 (Fig. S3).

For optical microscopy, the distance from replicate measurement j of aperture pair i is $D_{ij}^{OM} = \Delta_i + d_{ij}^{OM} + \delta_i^{OM}$, where Δ_i is the same true distance as in the fixed-effect linear model for atomic-force microscopy, d_{ij}^{OM} is a random error that is observable between replicate measurements of aperture pair i , and δ_i^{OM} is a random error that is unobservable in replicate measurements of aperture pair i .

Distance deviations between the two methods are $D_{i\cdot}^{OM} - D_{i\cdot}^{AFM} = \delta_i^{OM} + d_{i\cdot}^{OM} - \delta_i^{AFM} - d_{i\cdot}^{AFM}$, where the dot for j in the subscript denotes averaging over replicates. We denote the variance of $D_{i\cdot}^{OM} - D_{i\cdot}^{AFM}$ by $\sigma_{D_{OM-D_{AFM}}}^2$, the variance of δ_i^{AFM} by $\sigma_{\delta_{AFM}}^2$, the variance of δ_i^{OM} by $\sigma_{\delta_{OM}}^2$, the variance of $d_{i\cdot}^{AFM}$ by $\sigma_{d_{AFM}}^2/n_{D_{AFM}}$, and the variance of $d_{i\cdot}^{OM}$ by $\sigma_{d_{OM}}^2/n_{D_{OM}}$ (Table S1).

Autoregressive–moving-average model

In the fixed-effect linear model, we account for the fact that adjacent pairs of apertures share one aperture by assuming distinct distances for each pair. However, we might also assume a single mean distance for all pairs of apertures along an axis, but allow for autocorrelation between them. We

expect a negative autocorrelation between distance measurements of adjacent pairs, and we use an autoregressive–moving-average model [7] to allow and account for this effect. The model applies to averages across replicates but does not apply to the individual replicates (Fig. S3). The typical application of such a model is to a time series, whereas our measurement results have a spatial, rather than a temporal, distribution. Nonetheless, along each scan axis of the atomic force microscope, the spatial distribution is one-dimensional, neglecting off-axis effects of fabrication precision that are small, so that the model is still applicable. A negative autocorrelation is clearly present for axis 2, but is only faintly evident for axis 1 (Fig. S3). These results are consistent with the respectively lower and higher variability of replicate measurements along the scan axes (Fig. S3). Zero autocorrelation is a limiting case for autoregressive–moving-average models, so the same statistical methodology is applicable for both axes.

A challenge in applying the autoregressive–moving-average family of models is choosing a member. To this end, we apply the methodology of Ref. [8], using common software for statistical analysis [9]. For axis 1, this methodology selects a model that does not include autocorrelation, that is, a model that takes the distances to be statistically independent. For axis 2, the methodology selects a moving average model of order 1. To test these results, we simulate hypothetical values from the model selections for comparison to the measurement results (Fig. S3). The simulation and measurement results are in good agreement, implying that the selections of the methodology are fit for our purpose.

For axis 1, the mean distance is $5000.72 \text{ nm} \pm 0.21 \text{ nm}$, for axis 2 it is $5000.57 \text{ nm} \pm 0.19 \text{ nm}$, and for all 22 pairs, it is $5000.64 \text{ nm} \pm 0.14 \text{ nm}$. The estimate of diagonal distance is $77791.8 \text{ nm} \pm 2.5 \text{ nm}$. These results are in good agreement with the results of the fixed-effect linear model in the main text. In most cases, the 68 % coverage intervals from the autoregressive-moving-average models are slightly larger. This is because the autoregressive models incorporate aperture placement as an additional component of uncertainty into their assessments. The additional capability results from accounting for differences in distances through correlation effects of second order, instead of mean effects of first order.

Table S4. Distance uncertainty observability

Extent of observability	Component of uncertainty or variability
Observable between replicate measurements by AFM or OM	$\sigma_{d^{AFM}}^2, \sigma_{d^{OM}}^2$
Observable between correlative measurements by AFM and OM	$\sigma_{\delta^{AFM}}^2, \sigma_{\delta^{OM}}^2$
Unobservable between correlative measurements by AFM and OM	σ_S

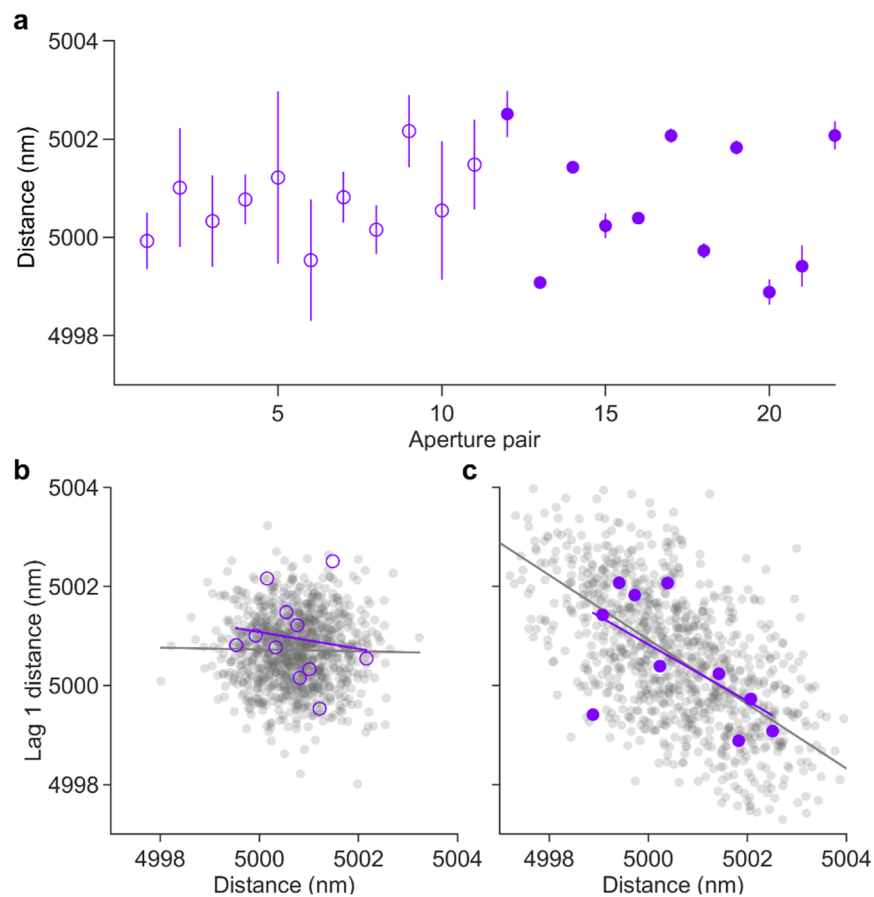


Fig. S3. Autocorrelation analyses. (a) Plot showing distance measurements along (hollow circles) axis 1 and (solid circles) axis 2 of the atomic force microscope. Uncertainties are 68 % coverage intervals from replicate measurements. (b, c) Plots showing autocorrelation analyses of distance measurements along (b) axis 1 and (c) axis 2. Vertical axes show lag 1 distances. Horizontal axes show distances between aperture pairs. Purple data points are measurement results. Purple lines are least-squares fits to measurement results. Gray data points are simulation results from the model selection. Gray lines are least-squares fits to simulation results. (c) A few gray data points lie outside of the plot range, which maximizes clarity. The variability of the data that is observable is one component of the total uncertainty. We subsequently propagate uncertainty of scale.

Table S5. Distance deviation variances

AFM axis	OM axis	$\sigma_{d^{AFM}}^2$ (nm ²)	$\sigma_{d^{AFM}}^2/n_{D^{AFM}}$ (nm ²)	$\sigma_{d^{OM}}^2$ (nm ²)	$\sigma_{d^{OM}}^2/n_{D^{OM}}$ (nm ²)	$\sigma_{D^{OM}-D^{AFM}}^2$ (nm ²)
1	y	1.86	0.62	0.28	0.00028	1.69
2	x	0.11	0.04	0.25	0.00025	0.78

Statistical variances of replicate measurements pool over aperture pairs for both microscopy methods.

Table S6. Distance uncertainty evaluation

Uncertainty component	Evaluation	Absolute value for x direction (nm)	Absolute value for y direction (nm)
$\sigma_{D^{OM}-D^{AFM}}$	Type A, measurement	0.89 ± 0.21	1.30 ± 0.31
$\sigma_{d^{AFM}}/\sqrt{n_{D^{AFM}}}$	Type A, measurement	0.19 ± 0.05	0.79 ± 0.19
$\sigma_{\delta^{AFM}}$	Type B, estimate	0.02	0.004
$\sigma_{d^{OM}}/\sqrt{n_{D^{OM}}}$	Type A, measurement	0.016 ± 0.004	0.017 ± 0.004
$\sigma_{\delta^{OM}}$	Type A, Eq. (3)	0.87 ± 0.13	1.03 ± 0.18
$\sigma_{\delta^{OM}}$	Type A, Reference [10]	0.88 ± 0.28	1.02 ± 0.27

The solution for $\sigma_{\delta^{OM}}$ depends on a Type B evaluation of $\sigma_{\delta^{AFM}}$, which would typically result in an overall categorization of a Type B evaluation for $\sigma_{\delta^{OM}}$. However, the effect of $\sigma_{\delta^{AFM}}$ is negligible, so that the solution for $\sigma_{\delta^{OM}}$ effectively involves only Type A evaluations of the three other components, resulting in an effective overall categorization of Type A.

Note S3. Distance uncertainty for optical microscopy

The Euclidean distance D^{OM} between two points in two lateral dimensions depends on the positions of the points in the x and y directions. In the main text, Eq. (4) describes the total uncertainty of position in a single lateral dimension for the case that one of the points is a reference position without localization uncertainty, so that the uncertainty for D_x^{OM} is $\sigma_{D_x^{OM}}/\sqrt{2}$,

$$u_{D_x^{OM}} = u_{D_x^{OM}}^I = \sqrt{\left(\sigma_{D_x^{OM}}/\sqrt{2}\right)^2 + \left(D_x^{OM} \times \sigma_S\right)^2}. \quad (\text{S1})$$

We denote whether one or two points are the result of localization analysis with corresponding uncertainty by superscript Roman numerals I and II, respectively. We omit this notation in the main text for concision. The division of $\sigma_{D_x^{OM}}$ by $\sqrt{2}$ is due to our quantification of $\sigma_{d^{OM}}$ and $\sigma_{\delta^{OM}}$ by measurements of distance between two points (Table S6), assuming equal localization uncertainty for each point.

We derive a general expression for the uncertainty of D^{OM} , for the case that the positions of both points are the result of localization analysis, $u_{D^{OM}}^{\text{II}}$ (Table S1). In this case, the uncertainty for D_x^{OM} is $\sigma_{D_x^{OM}}$ (Table S6). We express measurement equations that account for the relative uncertainty of scale σ_S through a multiplicative scale factor S , so that the distances in the x and y directions are the products SD_x^{OM} and SD_y^{OM} , respectively. By linearizing SD_x^{OM} and calculating the standard deviation of the resulting linear approximation, we determine an approximate uncertainty,

$$u_{D_x^{OM}}^{\text{II}} = \sqrt{\sigma_{D_x^{OM}}^2 + \left(D_x^{OM} \times \sigma_S\right)^2}, \quad (\text{S2})$$

which is Eq. (4) and Eq. (S1) without the factor $\frac{1}{\sqrt{2}}$ that converts the first term from a distance uncertainty to a position uncertainty. The Euclidean distance is then,

$$D^{OM} = S\sqrt{\left(D_x^{OM}\right)^2 + \left(D_y^{OM}\right)^2}. \quad (\text{S3})$$

Again, by linearizing D^{OM} and calculating the standard deviation of the resulting linear approximation, we arrive at an approximate expression for the uncertainty of D^{OM} ,

$$u_{D^{OM}}^{\text{II}} = \sqrt{\frac{\left(D_x^{OM}\right)^2 \sigma_{D_x^{OM}}^2 + \left(D_y^{OM}\right)^2 \sigma_{D_y^{OM}}^2}{\left(D_x^{OM}\right)^2 + \left(D_y^{OM}\right)^2} + \left(\left(D_x^{OM}\right)^2 + \left(D_y^{OM}\right)^2\right) \sigma_S^2}. \quad (\text{S4})$$

Eq. (S2) and Eq. (S4) are similar. In Eq. (S2), the first term is the square of the uncertainty for a single lateral dimension. In Eq. (S4), the first term is a weighted average of the square of the distance uncertainties for both lateral dimensions x and y . In both equations, the second term is the product of the square of the uncertainty of scale and the square of the distance between the points.

Table S7. Master and working standards

Aperture arrays						
Standard type	Master	Working	Working	Working	Working	Working
Array number	1	2	3	4	5	6
Lithography parameters						
Lithography system 1 or 2	1	1	2	2	2	2
Electron-beam distortion correction	yes	no	yes	yes	yes	yes
Electron-beam current (nA)	1.000	1.000	1.000	1.000	0.125	0.200
Exposure passes	1	1	1	1	8	1
Microscopy results						
Mean pitch (nm)	5000.71	4999.90	5000.30	5001.45	4997.30	4996.44
Standard error of the mean (nm)	0.13	0.03	0.01	0.03	0.08	0.08
Degrees of freedom	43	2	4	5	2	2
Traceable uncertainty (nm)	0.54	0.54	0.54	0.54	0.54	0.54

Lithography system 1 has a write field of 62.5 μm by 62.5 μm and a beam placement specification of 0.125 nm.

Lithography system 2 has a write field of 1 mm by 1 mm and a beam placement specification of 2 nm.

Note S4. Lithographic pitch accuracy

To test the accuracy of lithographic pitch, we use critical-dimension localization microscopy to measure the pitch variability of the master aperture array from the main text, along with five additional aperture arrays that serve as working standards. All six arrays have a nominal pitch of 5000 nm. In the electron-beam lithography process, we vary the current of the electron beam and the number of exposure passes while keeping the total dose constant (Table S7). Further details of the overall process of nanofabrication are in Supplemental Reference [10].

Array 2 consists of a single substrate with three different arrays of 12 apertures by 12 apertures that we image, while arrays 3 through 6 are single arrays with lateral extents of 300 μm from which we image multiple distinct subsets of 12 apertures by 12 apertures. We localize the aperture positions in each image. A similarity transformation between the aperture positions and those of the master aperture array determines a multiplicative scale factor relating the traceable pitch of the master standard to the pitch of each working standard (Table S7).

A statistical meta-analysis [11] characterizes the variability of pitch across the arrays, taking as inputs the mean value of pitch and its standard error for each array (Table S3). This consensus analysis determines a dark uncertainty of 2.25 nm, which we interpret as a measure of pitch variability due to variation of the lithography process, and a consensus mean value of pitch with a coverage interval that we expand by propagating the total uncertainty of scale (Table S3) by Monte-Carlo methods, yielding a traceable value of 4999.34 nm \pm 1.00 nm. We apply the uncertainty of scale after the consensus analysis, as this uncertainty would otherwise obscure the estimate of dark uncertainty. Finally, this analysis yields a prediction interval of 4999.40 nm \pm 2.34 nm for additional aperture arrays. We interpret this prediction interval as a conservative estimate of the reliability of producing working standards, due to our deliberate variation of lithographic process parameters.

References

1. B. N. Taylor and C. E. Kuyatt, NIST Technical Note **1297** (1994).
2. Joint Committee for Guides in Metrology, JCGM **100** (2008).
3. A. Possolo, NIST Technical Note **1900** (2015).
4. R. E. Thompson, D. R. Larson, and W. W. Webb, Biophysical Journal **82**, 2775-2783 (2002).
5. K. I. Mortensen, L. S. Churchman, J. A. Spudich, and H. Flyvbjerg, Nature Methods **7**, 377-381 (2010).
6. S. Ahn and J. A. Fessler, EECS Department, The University of Michigan, 1-2 (2003).
7. W. A. Fuller, *Introduction to statistical time series* (John Wiley & Sons, 2009).
8. R. J. Hyndman and Y. Khandakar, Journal of Statistical Software **27**, 1-22 (2008).
9. R. C. Team, R: A language and environment for statistical computing, R Foundation for Statistical Computing, Vienna, Austria, (2013).
10. C. R. Copeland, J. Geist, C. D. McGray, V. A. Aksyuk, J. A. Liddle, B. R. Ilic, and S. M. Stavis, Light: Science & Applications **7**, 1-15 (2018).
11. A. Koepke, T. Lafarge, A. Possolo, and B. Toman, Metrologia **54**, S34 (2017).